



HAL
open science

Dc-bias-field-induced Dielectric Relaxation and AC Conduction in $\text{CaCu}_3\text{Ti}_4\text{O}_{12}$ Ceramics

Laijun Liu, Huiqing Fan, Lei Wang, Xiuli Chen, Pinyang Fang

► **To cite this version:**

Laijun Liu, Huiqing Fan, Lei Wang, Xiuli Chen, Pinyang Fang. Dc-bias-field-induced Dielectric Relaxation and AC Conduction in $\text{CaCu}_3\text{Ti}_4\text{O}_{12}$ Ceramics. *Philosophical Magazine*, 2008, 88 (04), pp.537-545. 10.1080/14786430801894551 . hal-00513860

HAL Id: hal-00513860

<https://hal.science/hal-00513860v1>

Submitted on 1 Sep 2010

HAL is a multi-disciplinary open access archive for the deposit and dissemination of scientific research documents, whether they are published or not. The documents may come from teaching and research institutions in France or abroad, or from public or private research centers.

L'archive ouverte pluridisciplinaire **HAL**, est destinée au dépôt et à la diffusion de documents scientifiques de niveau recherche, publiés ou non, émanant des établissements d'enseignement et de recherche français ou étrangers, des laboratoires publics ou privés.



Dc-bias-field-induced Dielectric Relaxation and AC Conduction in CaCu₃Ti₄O₁₂ Ceramics

Journal:	<i>Philosophical Magazine & Philosophical Magazine Letters</i>
Manuscript ID:	TPHM-07-Oct-0299.R1
Journal Selection:	Philosophical Magazine
Date Submitted by the Author:	07-Dec-2007
Complete List of Authors:	Liu, Lajun; Ecole Centrale Paris, Laboratoire SPMS, UMR8580 CNRS; Northwestern Polytechnical University, School of Materials Science and Engineering Fan, huiqing; Northwestern Polytechnical University Wang, Lei; Northwestern Polytechnical University; Northwestern Polytechnical University Chen, Xiuli; Northwestern Polytechnical University Fang, Pinyang; Northwestern Polytechnical University
Keywords:	electronic properties, ferroelectrics, functional materials, grain boundary interfaces, hopping conduction, perovskites, titanium oxide
Keywords (user supplied):	Dielectric relaxation, Grain boundary, Impedance spectroscopy



Dc-bias-field-induced Dielectric Relaxation and AC Conduction in $\text{CaCu}_3\text{Ti}_4\text{O}_{12}$ Ceramics

Laijun Liu, Huiqing Fan*, Lei Wang, Xiuli Chen and Pinyang Fang

State Key Laboratory of Solidification Processing, School of Materials Science and Engineering, Northwestern Polytechnical University, Xi'an 710072, China

Abstract

The dielectric relaxation and ac conduction of $\text{CaCu}_3\text{Ti}_4\text{O}_{12}$ (CCTO) ceramics were investigated at different temperatures under a dc bias. The dc biases give rise to the space charges accumulating, namely electrode response, resulting in the significant increase of dielectric permittivity and dielectric loss tangent. Two Debye-like relaxations, arising from both electrode and grain boundary response, present in low frequency with the increase of the dc biases. The electrode relaxation and grain boundary relaxation are distinguished according to the impedance spectroscopy and the frequency dependent ac conductivity. The relaxation time of electrode and grain boundary is 0.955 ms and 0.026 ms with a dc bias of 10 V at 328 K, respectively.

Keywords: Dielectric relaxation; Grain boundary; Impedance spectroscopy

PACS number(s): 77.22.Ch, 77.84.Dy

* Author to whom correspondence should be addressed; electronic mail: hqfan3@163.com

1. Introduction

1
2
3
4
5
6
7
8
9
10
11
12
13
14
15
16
17
18
19
20
21
22
23
24
25
26
27
28
29
30
31
32
33
34
35
36
37
38
39
40
41
42
43
44
45
46
47
48
49
50
51
52
53
54
55
56
57
58
59
60

Miniaturizing capacitor devices is demanding for higher dielectric permittivity materials progressively. In recent years, many researches have shown that the perovskite structure calcium copper titanate, $\text{CaCu}_3\text{Ti}_4\text{O}_{12}$ (CCTO), possesses a giant dielectric permittivity of 10^5 at room temperature, which is practically frequency independent between dc and 10^6 Hz. In addition, this material does not show ferroelectric transition in a wide temperature range (100-600 K), where the dielectric permittivity value remains constant, without suffering from limitations of commonly used ferroelectric materials.¹⁻⁶ The dielectric permittivity abruptly drops down to a value, ~ 100 when the temperature lowers below 100 K.^{7,8} The dielectric response behavior of the material is characteristic of Debye-like relaxation with a single relaxation time.⁹

A number of attempts to interpret this behavior in terms of intrinsic material properties^{10,11} as well as an impurity and interface mediated phenomena¹² have been reported. One of the leading explanations for giant dielectric permittivity is the formation of nonconductive grain boundaries between conductive grains, i.e., grain-boundary layer capacitor behavior, common in doped perovskite titanates.¹³ This model was supported by impedance spectroscopy.¹⁴⁻¹⁶ Recently, however, it is reported that the giant dielectric permittivity is associated with electrode polarization effects due to nonohmic contacts but not due to a grain boundary effect.¹⁷ Such nonohmic electrode contacts are well known to occur with many different types of materials due to their different electron work functions. The interface polarization

1
2
3
4 behavior, termed Maxwell-Wagner relaxation, has been observed in many materials.
5
6
7 Generally, the electrode effects can be well separated by using different contacts and
8
9
10 sample geometries.¹⁸ However, few researchers attempted to separate electrode effect
11
12 from grain boundary effect. Up to now it is still unclear that which effect is
13
14 responsible for the giant dielectric permittivity in CCTO. This question may be
15
16 resolved if the two responses, electrode relaxation and grain boundary relaxation, can
17
18 be distinguished.
19
20
21

22
23 In this work, the measurement of dielectric and impedance spectroscopy of
24
25 CCTO ceramics is reported in the temperature range from 298 K to 358 K at 0, 5, 10,
26
27 15, 20 and 40 V dc bias. A low frequency dielectric relaxation arising from electrode
28
29 polarization was induced by dc bias. The electrode response and grain boundary
30
31 response have been successfully distinguished from each other according to
32
33 impedance spectroscopy and the frequency dependent ac conductivity with a dc bias.
34
35 Each component acts as a depletion layer to induce their own respective dielectric
36
37 relaxations.
38
39
40
41
42

43 44 **2. Experiment**

45
46 Reagent grade oxides and nitrates, $\text{Ca}(\text{NO}_3)_2 \cdot 4\text{H}_2\text{O}$, $\text{Cu}(\text{NO}_3)_2 \cdot 3\text{H}_2\text{O}$ and TiO_2
47
48 and sodium potassium chloride ($\text{NaCl} : \text{KCl} = 44 : 56$) were used as the starting
49
50 materials. Appropriate amounts of the oxide and chloride powders were mixed
51
52 together in the ball mill using zirconia balls as milling medium in ethanol for 12 h.
53
54 The dried powder mixtures were placed in covered high alumina crucibles, and then
55
56 heated in a chamber furnace at 800°C for 1 hour. On the completion of reaction, flux
57
58
59
60

1
2
3
4 salt was removed from the powder particles by repeated washing with hot deionized
5
6 water until no chloride ions were detected by silver nitrate. The obtained CCTO
7
8 powder was pressed into pellets of 15 mm diameter and ~1 mm thickness by cold
9
10 isostatic pressure method. The pellets were sintered at 1060°C in air for 48 hours.
11
12 X-ray diffraction patterns were obtained using an automated diffractometer (XRD;
13
14 X'Pert PRO MPD, Philips, Eindhoven, Netherlands) with Cu $K\alpha_1$ radiation. The
15
16 surface morphologies of CCTO ceramics were observed by a scanning electron
17
18 microscope (SEM; JSM-5610, JEOL, Tokyo, Japan). Both sides of the samples were
19
20 polished and then brushed with silver conductive paste followed by heat treatment at
21
22 550°C for 30 minutes in order to ensure good electrical contact. Electrical properties
23
24 measurements were taken with an applied voltage of 500 mV using an Agilent 4294A
25
26 impedance analyzer over the frequency range 100 Hz–13 MHz at room temperature
27
28 and 100 Hz- 100 kHz at selected temperatures between 298 K and 358 K at 0, 5, 10,
29
30 15, 20 and 40 V dc.
31
32
33
34
35
36
37
38
39
40

41 3. Results and discussion

42
43 Figure 1 shows typically the room-temperature XRD pattern for the CCTO
44
45 ceramics sintered at 1060°C. The diffraction peaks could be indexed by a
46
47 body-centered cubic perovskite-related structure of space group Im3 according to
48
49 ICSD 032002. Fig. 2 shows the SEM images of surface morphology of molten salt
50
51 derived CCTO ceramics. The average grain size of our sample is about 8 μm . The
52
53 grain size of the ceramics is uniform and the grain boundary is clean. It indicates that
54
55 the specimen prepared in the present study have a good polycrystalline structure.
56
57
58
59
60

1
2
3
4 The frequency dependence of the real part and imaginary part of dielectric
5 permittivity of CCTO ceramics at 0 V, 5V, 10V, 15 V and 20 V dc bias at room
6 temperature is shown in Fig. 3. The real part of dielectric permittivity with no dc bias
7 is ~100,000 over a wide frequency range between 100 Hz and 7 MHz. And it
8 enhances sharply with the increase of dc bias in low frequency (< 3 kHz), but an
9 inverse change happens in high frequency (> 10 kHz, Fig. 3 inset). Two Debye-like
10 relaxations present in the imaginary of dielectric permittivity, one is in $10^6\sim 10^7$ Hz
11 associating with grain/domain response; the other is below 100 Hz associating with
12 grain boundary response and/or electrode response. Admas *et al.*¹⁶ found that the
13 capacitance of grain boundary decreases with bias increasing. This is consistent with
14 the expectation of a Schottky barrier model for the grain boundary with a reduction in
15 potential barrier height in the forward bias direction and an increase in the width of
16 depletion region. The dielectric-dc bias behavior of CCTO ceramics is consonant with
17 this result in high frequency range. However, the low frequency dc-bias-field-induced
18 dielectric relaxation is very interesting.

19
20
21
22
23
24
25
26
27
28
29
30
31
32
33
34
35
36
37
38
39
40
41
42
43
44 Nonohmic electrode contacts always occur with many different types of
45 materials due to their different electron work functions and electrode contact
46 conditions and that surface roughness and wetting. The electrode polarization at the
47 interface between the sample and electrode, like grain boundary response, may be one
48 of the sources of the giant dielectric permittivity. In the following we will adopt the
49 view that the change of dielectric permittivity in low frequency range is mainly arisen
50 from external contacts. It is well known that thin depletion layers can arise, e.g., due
51
52
53
54
55
56
57
58
59
60

1
2
3
4 to the formation of Schottky diodes at the electrode/bulk interface.¹⁹ These thin layers
5
6 of low conductivity act as high capacitance in parallel with a very large resistor,
7
8 connected in series to the bulk, which can results in the erroneous detection is very
9
10 large values of dielectric permittivity. Under the suitable conditions like application of
11
12 a static bias across the sample, a pile of these low mobility charge carriers is collected
13
14 around one of blocking electrode. This leads to a field gradient near the electrode and
15
16 gives rise to a non-linear dielectric permittivity and loss tangent. Considering the
17
18 blocking nature of the electrodes, two relaxation peaks should be observed,
19
20 unfortunately, we can not find two complete peaks in Fig. 3. **The reason is the**
21
22 **measurement limit of our impedance analyzer. We can not obtain a high temperature**
23
24 **and a wide range frequency.** We will detect them by impedance spectroscopy.
25
26
27
28
29
30
31
32

33 Z^* plot of data obtained of CCTO ceramics with a dc bias of 0 V (a) and 10 V (b)
34
35 at different temperatures are shown in Fig. 4. The resistances of grain and grain
36
37 boundary decrease with the increase of temperature and dc bias. A large arc with
38
39 nonzero intercept at high frequency ($> 10^6$ Hz) is shown in Fig. 4a and inset. Only a
40
41 small section of the grain boundary arc can be observed at low temperature, and a
42
43 steep incline at low frequency suggests that the resistance of grain boundary is much
44
45 more than $10^5 \Omega\text{-cm}$ and its response frequency is less than 100 Hz. The grain
46
47 boundary response and electrode response are still not distinguished. An impedance
48
49 spectroscopy of CCTO ceramics with a dc bias of 10 V is shown in Fig. 4b and right
50
51 inset. Both grain boundary resistance and grain resistance decrease with the increase
52
53 of dc bias and temperature, which is consistent with a Schottky barrier response. The
54
55
56
57
58
59
60

left inset in Fig. 4b shows the measuring impedance spectroscopy and calculating impedance spectroscopy according to an equivalent circuit, a series circuit of parallel RC elements. The impedance attributing to grain and grain boundary is calculated by Eq. 1 (Grain resistance $R_g = 135.27 \Omega$, grain capacitance $C_g = 17.4 \text{ nF}\cdot\text{cm}$, grain boundary resistance $R_{gb} = 5375.48 \Omega$ and grain boundary capacitance $C_{gb} = 80.49 \text{ nF}\cdot\text{cm}$). Here shows a semicircular arc with its center lying underneath the abscissa. In comparison with Z^* plot data, here the impedance changes from electrode relaxation to grain boundary relaxation as frequency increases beyond $f = 19 \text{ kHz}$ at 328 K with a dc bias of 10 V , as indicated by an arrow. The relaxation time of electrode and grain boundary is 0.955 ms and 0.026 ms with a dc bias of 10 V at 328 K , respectively. It is clear that the impedance responses from grain boundary and electrode are convoluted in the semicircular arc even if both measuring temperature and dc bias increase.

$$Z = R + jX = \frac{R_g}{1 + \omega^2 R_g^2 C_g^2} + \frac{R_{gb}}{1 + \omega^2 R_{gb}^2 C_{gb}^2} - j \left(\frac{\omega R_g^2 C_g}{1 + \omega^2 R_g^2 C_g^2} + \frac{\omega R_{gb}^2 C_{gb}}{1 + \omega^2 R_{gb}^2 C_{gb}^2} \right) \quad (1)$$

To further corroborate our findings, we also research the ac conductivity of CCTO ceramics. The bulk dc conductivity follows a variable-range-hopping mechanism under which the bulk ac conductivity also obeys a power law. This has been attributed to polaron relaxation, a phenomenon widely recognized in defective perovskite structure at low temperature. The frequency dependence on the ac conductivity σ at different temperatures is shown in Fig. 5a. The conductivity almost presents a step for $T = 358 \text{ K}$ at low frequency, as marked by ellipse, which is approximately equal to the dc electrode conductivity σ_e . The step is very short because

the temperature is low and the lowest measurement frequency is still high. As seen from these lines, the conductivity of them increase rapidly starting at frequency $f \sim 100$ Hz, beyond which the σ can be described as

$$\sigma = \sigma_{gb} + a_1 f^t + \alpha f^2 \quad (2)$$

where σ_{gb} is the dc grain boundary conductivity, a_1 , t and α are three adjustable constants. In this formula, the $\sigma_{gb} + a_1 f^t$ term describes the grain boundary conductivity relaxation. The conductivity of CCTO ceramics changes from the grain boundary response to the grain conductivity (domain conductivity) with the increase of frequency. The αf^2 term describes approximately the transition between the above two mentions relaxation behaviors.

A dc bias of 20 V is loaded on CCTO ceramics in order to find electrode relaxation clearly. Fig. 5b shows the frequency dependence on the ac conductivity σ at 298 K and 348 K. A long plateau presents in low frequency, associating with the dc electrode conductivity σ_e . As the frequency f is increased to inflexion, σ also increases as a result of electrode conductivity relaxation as described by

$$\sigma = \sigma_e + a_2 f^s \quad (3)$$

where a_2 and s ($0 < s \leq 1$) are two temperature dependent adjusting constants. The $a_2 f^s$ term is an empirical expression representing the transport properties of polarons, electrons, and ions.²⁰

The solid lines are the fitting curves according to Eq. (2) in Fig. 5a. With an absence of dc bias, it is not clear that the conductivity changes from electrode relaxation to grain boundary relaxation. Maybe it happens in very low frequency.

However, α increases from negative value to positive value (from -5.75×10^{-12} to 3.66×10^{-12} S/cm), suggesting that the relationship between grain relaxation and grain boundary becomes closer with the increase of temperature. The activation energies of the aforementioned electrical responses from grains and grain boundaries are calculated. The activation energy is associated with the height of the potential-energy barrier restricting the motion of charge carriers. Conductivities of the grain (bulk), σ_b , and grain boundary, σ_{gb} , components are obtained and plotted against reciprocal temperature in Arrhenius format.

$$\sigma = \sigma_0 \exp\left(\frac{E_a}{k_B T}\right) \quad (4)$$

where σ_0 is the prefactor, E_a is the activation energy for the relaxation, k_B is the Boltzmann constant, and T is the absolute temperature. Fig. 5a inset shows the plot of $\log \sigma$ versus $1/T$, in which the solid line is fitted result using Eq. 4. Both obey the Arrhenius law with grain activation energies of 0.122 eV and grain boundary activation energies of 0.40 eV with an absence of dc bias.

The dot lines (1 and 3) are the fitting curves according to Eq. (3) and the solid lines (2 and 4) are the fitting curves according to Eq. (2) in Fig. 5b. The coefficients of fitting formulas are shown in Table I. The electrode conductivity increases from 1.10×10^{-6} S/cm to 1.74×10^{-4} S/cm as dc bias increases from 0 V to 20 V at 358 K. Also, the grain boundary conductivity increases with the increases of temperature and dc bias (Fig. 4 and 5). This reveals the strong electric field dependent nature of both electrode conductivity and grain boundary conductivity. Meanwhile, it is considered the conductivity is associated with electrode polarization effects and the development

1
2
3
4 of Schottky barriers at the metal electrode/ceramic interface due to nonohmic contacts
5
6
7 and grain boundaries effect.

8
9 At recent, Zhu et al.²¹ claimed the existence of nanoscale disorder of Cu/Ca
10 makes a remarkable effect on the dielectric properties of CCTO. A metalliclike
11 polarizability in the surrounding insulating regions enhances dynamical electronic
12 dielectric response. This mechanism is different from the “internal barrier layer
13 capacitor” (IBLC) picture. It may be the origin of giant dielectric constant in CCTO
14 single crystal and grains in CCTO ceramics. However, in CCTO polycrystals,
15 impedance spectroscopy and dielectric constant dependence of electrodes also show
16 grain boundaries and electrode playing some important roles in giant dielectric
17 constant.^{16, 17} In this work, our focus is the influence of grain boundaries and electrode
18 on dielectric response.

35 36 **4. Conclusions**

37
38 CCTO ceramics fired silver electrodes were measured at different temperatures
39 with a dc bias. The dependence of dielectric permittivity on dc bias clearly proves that
40 the electrode causing an interfacial polarization process results in the detection of very
41 strong dc-bias-field-induced dielectric relaxation. The electrode relaxation is
42 separated distinctly from grain boundary relaxation via an understandable equivalent
43 circuit calculating according to impedance spectroscopy under a dc bias. The
44 electrode and grain boundary act as two depletion layers. Both of them make a great
45 contribution to the ac conductivity of CCTO ceramics.

56 57 58 59 60 **Acknowledgements**

1
2
3
4 This work has been supported by the National Nature Science Foundation (50672075)
5
6
7 and the Xi'an S&T Research Foundation (GG05015, GG06023), the SRFDP
8
9
10 (20050699011) and EYTP and NCET Program of MOE, Doctorate Foundation
11
12 (CX200704) and Science Creative Foundation (2006CR06) NPU of China.
13
14
15
16
17
18
19
20
21
22
23
24
25
26
27
28
29
30
31
32
33
34
35
36
37
38
39
40
41
42
43
44
45
46
47
48
49
50
51
52
53
54
55
56
57
58
59
60

For Peer Review Only

Reference

- [1] B. G. Kim, S. M. Cho, T. Y. Kim, and H. M. Jang, *Phys. Rev. Lett.* 86 (2001), 3404.
- [2] J. B. Wu, C. W. Nan, Y. H. Lin, and Y. Deng, *Phys. Rev. Lett.* 89 (2002), 217601.
- [3] I. Vrejoiu, J. D. Pedarnig, D. Bäuerle, and M. Dinescu, *Appl. Phys. Lett.* 83 (2003), 2130.
- [4] A. P. Ramirez, M. A. Subramanian, M. Gardel, G. Blumberg, D. Li, T. Vogt, and S. M. Shapiro, *Solid State Commun.* 115 (2000), 217.
- [5] Y. Lin, Y. B. Chen, T. Garret, S. W. Liu, C. L. Chen, L. Chen, R. P. Bontchev, A. Jacobson, J. C. Jiang, E. I. Meletis, J. Horwitz, and H.-D. Wu, *Appl. Phys. Lett.* 81 (2002), 631.
- [6] D. C. Sinclair, T. B. Adams, F. D. Morrison, and A. R. West, *Appl. Phys. Lett.* 80, 2153 (2002).
- [7] M. A. Subramanian, D. Li, N. Duan, B. A. Reisner, and A. W. Sleight, *J. Solid State Chem.* 151 (2000), 323.
- [8] C. C. Homes, T. Vogt, S. M. Shapiro, S. Wakimoto, and A. P. Ramirez, *Science* 293 (2001), 673.
- [9] A. Tselev, C. M. Brooks, S. M. Anlage, H. Zheng, L. Salamanca-Riba, R. Ramesh, M. A. Subramanian, *Phys. Rev. B* 70 (2004), 144101.
- [10] L. He, J. B. Neaton, D. Vanderbilt, and M. H. Cohen, *Phys. Rev. B* 67 (2003), 012103.

- 1
2
3
4 [11] L. He, J. B. Neaton, M. H. Cohen, D. Vanderbilt, and C. C. Homes, Phys. Rev.
5
6 B 65 (2002), 214112.
7
8
9 [12] M. H. Cohen, J. B. Neaton, L. He, and D. Vanderbilt, J. Appl. Phys. 94 (2003),
10
11 3299.
12
13 [13] L. L. Hench and J. K. West, Principles of Electronic Ceramics, Wiley, New
14
15 York, 1990.
16
17 [14] T. T. Fang and H. K. Shiao, J. Am. Chem. Soc. 87 (2004), 2072.
18
19 [15] T. B. Adams, D. C. Sinclair, and A. R. West, Adv. Mater. (Weinheim, Ger.) 14
20
21 (2002), 1321.
22
23 [16] T. B. Adams, D. C. Sinclair, and A. R. West, Phys. Rev. B 73 (2006), 094124.
24
25 [17] P. Lunkenheimer, R. Fichtl, S. G. Ebbinghaus, and A. Loidl, Phys. Rev. B 70
26
27 (2004), 172102.
28
29 [18] P. Lunkenheimer et al., Phys. Rev. B 66 (2002), 052105.
30
31 [19] P.A. Miles et al., Rev. Mod. Phys. 29 (1957), 279.
32
33 [20] S. R. Elliott, Adv. Phys. 36 (1987), 135.
34
35 [21] Y. Zhu, J. C. Zheng, L. Wu, A. I. Frenkel, J. Hanson, P. Northrup, and W. Ku,
36
37 Phys. Rev. Lett. 99 (2007), 037602.
38
39
40
41
42
43
44
45
46
47
48
49
50
51
52
53
54
55
56
57
58
59
60

TABLE AND FIGURE CAPTIONS

TABLE I. Conductivity and temperature-dependent adjusting constants of Eq. (2) and (3) in the fitting curves.

FIG. 1. XRD pattern of molten salt derived CCTO ceramics.

FIG. 2. SEM image of molten salt derived CCTO ceramics.

FIG. 3. Dielectric permittivity of CCTO ceramics as a function with different dc biases at room temperature. Debye-like relaxations present in low frequency with the increase of dc bias.

FIG. 4. Impedance complex plane plot obtained for CCTO ceramics with a dc bias 0 V (a) and 10 V (b) at different temperatures. The right insets show an expanded view of the high frequency data close to the origin in (a) and (b). The left inset in (b) shows the calculated and measured impedance complex plane plots for CCTO ceramics with an absence of dc bias. The change from electrode relaxation to grain boundary relaxation is about 19 kHz, as indicated by an arrow. The relaxation time of electrode and grain boundary is 0.955 ms and 0.026 ms, respectively. Filled symbols indicate selected frequencies.

FIG. 5. (a) Frequency dependence of conductivity with an absence of dc bias at different temperatures. The solid lines are the fittings according to Eq. (2). The zone of ring marked shows the fitting is not good, suggesting a electrode response appearing in low frequency. The inset in (a) shows the Arrhenius plots of grain and grain boundary conductivity vs. temperature

1
2
3
4 for CCTO ceramics with an absence of dc bias. And (b) the frequency
5
6
7 dependence of conductivity with a dc bias of 20 V at 298 K and 348 K.
8
9
10 The solid lines 2 and 4 are the fitting according to Eq. (2), while the dot
11
12
13 lines 1 and 3 are the fitting according to Eq. (3).
14
15
16
17
18
19
20
21
22
23
24
25
26
27
28
29
30
31
32
33
34
35
36
37
38
39
40
41
42
43
44
45
46
47
48
49
50
51
52
53
54
55
56
57
58
59
60

For Peer Review Only

TABLE I

Condition	σ_{gb}	a_1	t	α	σ_e	a_2	s
Dc 0 V at 298K	-6.88	1.055	0.134	-5.75×10^{-12}			
Dc 0 V at 338K	-6.723	1.332	0.102	3.66×10^{-12}			
Dc 0 V at 358K	-5.96	1.016	0.107	2.54×10^{-12}			
Dc 20 V at 298K	-9.6	2.89	0.084	-7.32×10^{-11}	-4.76	0.005	0.643
Dc 20 V at 348K	-6.9	1.478	0.095	-1.16×10^{-12}	-3.76	0.179	0.085

For Peer Review Only

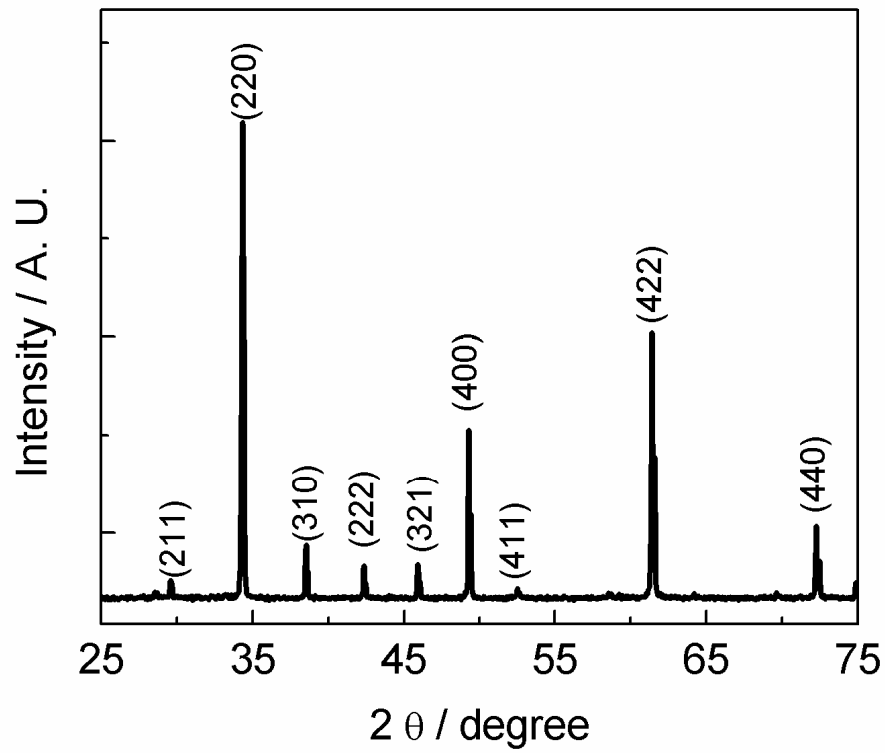
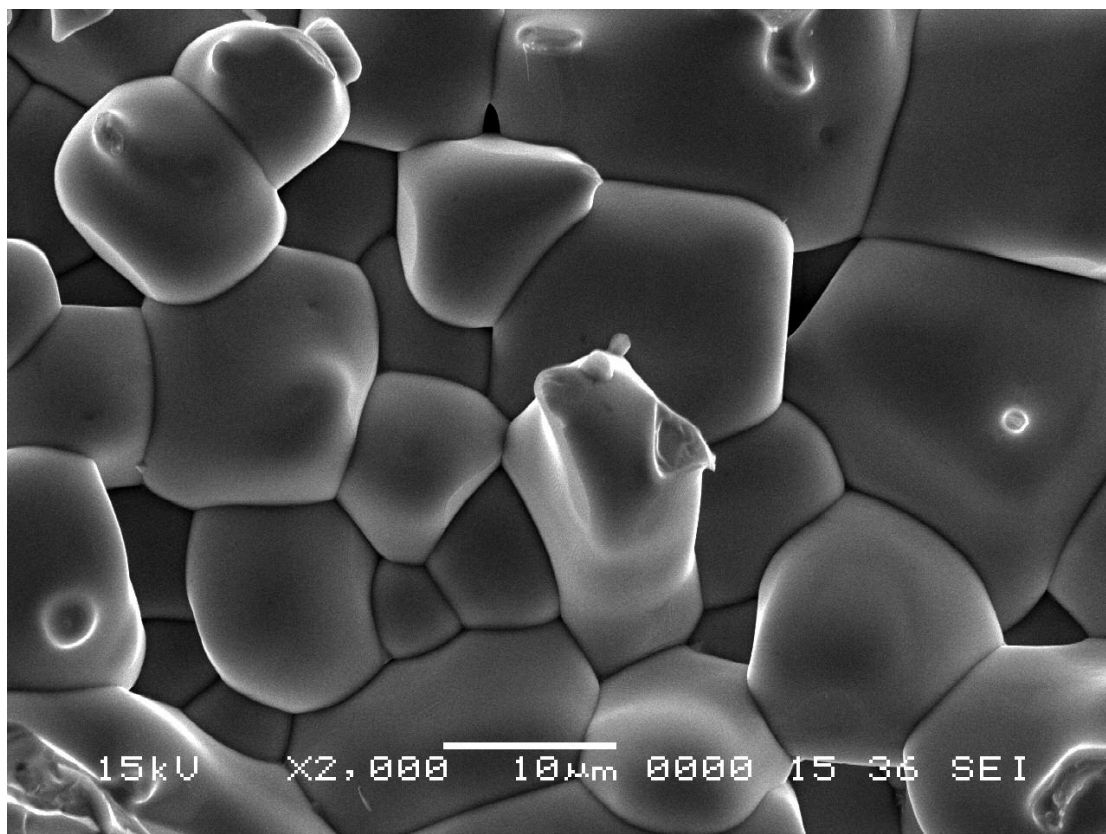


Figure 1



Review Only

Figure 2

1
2
3
4
5
6
7
8
9
10
11
12
13
14
15
16
17
18
19
20
21
22
23
24
25
26
27
28
29
30
31
32
33
34
35
36
37
38
39
40
41
42
43
44
45
46
47
48
49
50
51
52
53
54
55
56
57
58
59
60



Figure 3

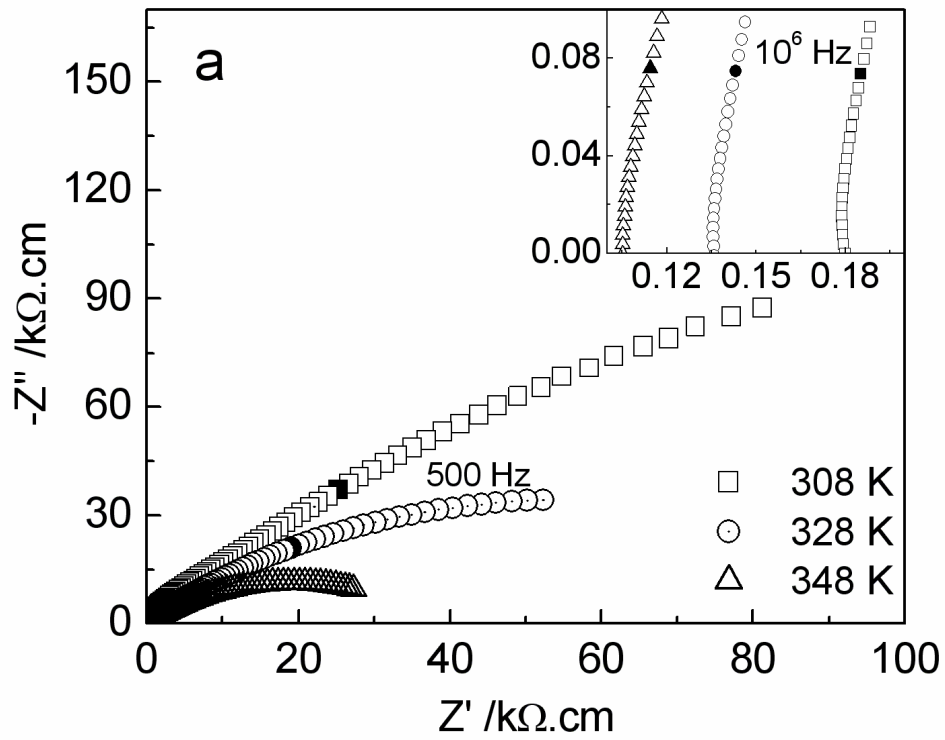


Figure 4a

1
2
3
4
5
6
7
8
9
10
11
12
13
14
15
16
17
18
19
20
21
22
23
24
25
26
27
28
29
30
31
32
33
34
35
36
37
38
39
40
41
42
43
44
45
46
47
48
49
50
51
52
53
54
55
56
57
58
59
60



Figure 4b

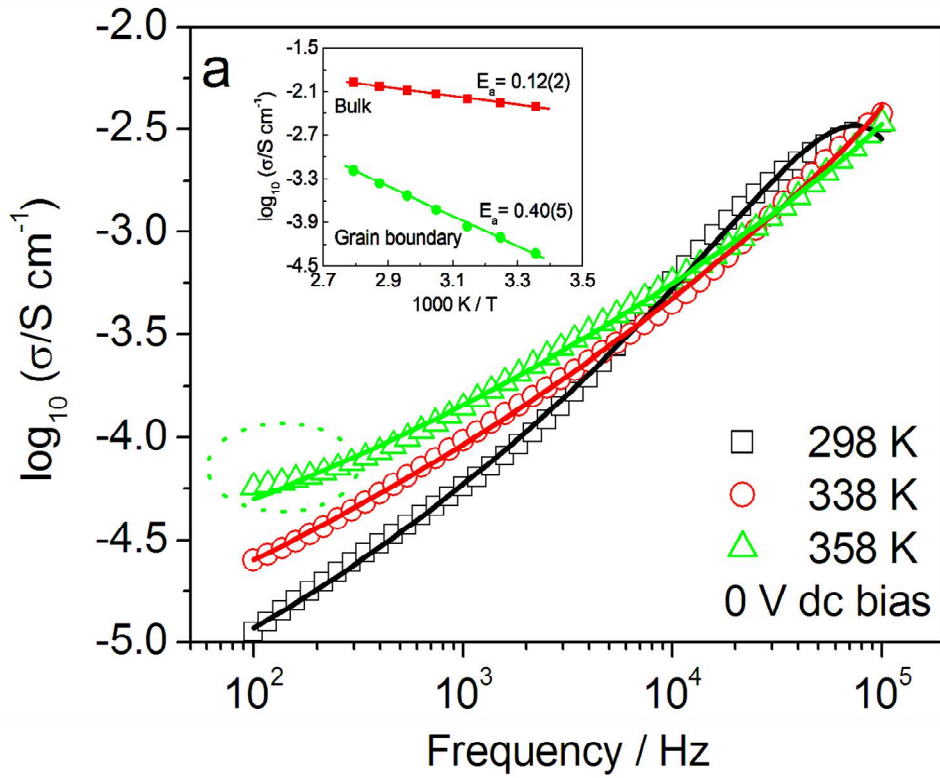


Figure 5a

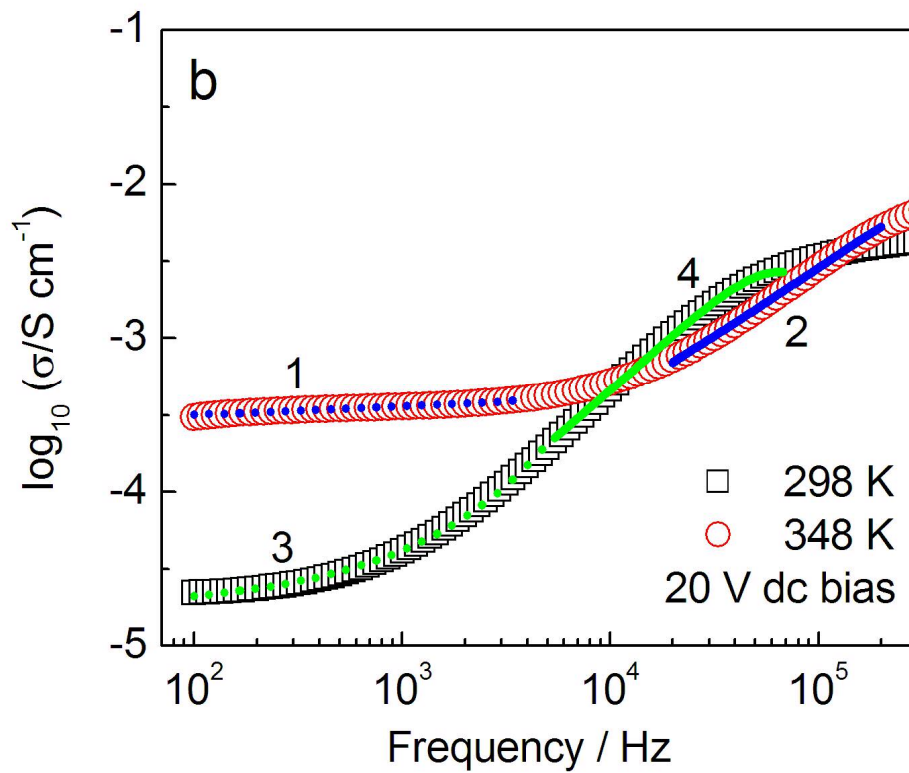


Figure 5b